AGU ADVANCING EARTH AND SPACE SCIENCES

JGR Solid Earth

RESEARCH ARTICLE
10.1029/2025JB033723

The 2024 Mw4.8 New Jersey Intraplate Earthquake: Preferential Rupture of an Immature Fault in Frictionally Unstable Basement Rocks

F. Kolawole[1,2], E. Beaucé[2], Z. Foster-Baril[2], M. Colet[1], L. Seeber[2], J. Tielke[2], A. Prakash[2], W. Y. Kim[2], R. Ajala[2], C. McCarthy[2], and F. Waldhauser[1,2]

[1]Department of Earth and Environmental Sciences, Columbia University, New York, NY, USA, [2]Lamont-Doherty Earth Observatory, Columbia University, New York, NY, USA

Key Points:

- Up-dip projection of aftershocks aligns with LiDAR traces of a basement fault zone with poorly coalesced shear fracture clusters
- Friction tests on fault rocks and slip tendency analysis of mapped slip planes predict fault instability at observed hypocentral depths
- This and other structurally studied seismic sources in the region manifest the hazards of prestressed, immature, subtle intraplate faults

Supporting Information:

Supporting Information may be found in the online version of this article.

Correspondence to:

F. Kolawole,
fola@ldeo.columbia.edu

Citation:

Kolawole, F., Beaucé, E., Foster-Baril, Z., Colet, M., Seeber, L., Tielke, J., et al. (2026). The 2024 Mw4.8 New Jersey intraplate earthquake: Preferential rupture of an immature fault in frictionally unstable basement rocks. *Journal of Geophysical Research: Solid Earth*, *131*, e2025JB033723. https://doi.org/10.1029/2025JB033723

Received 5 JAN 2026
Accepted 25 JUL 2026

Author Contributions:

Conceptualization: F. Kolawole, L. Seeber, W. Y. Kim
Data curation: F. Kolawole
Formal analysis: F. Kolawole, E. Beaucé, M. Colet, J. Tielke, A. Prakash
Funding acquisition: F. Kolawole, F. Waldhauser
Investigation: F. Kolawole, E. Beaucé, Z. Foster-Baril, M. Colet, L. Seeber, J. Tielke, A. Prakash
Methodology: F. Kolawole, E. Beaucé, L. Seeber, J. Tielke, C. McCarthy, F. Waldhauser
Project administration: F. Kolawole, F. Waldhauser
Resources: F. Kolawole, F. Waldhauser

Abstract Intraplate regions commonly host energetic earthquakes on less-prominent faults, raising questions on how fault structure may influence intraplate seismogenesis. We investigate the causative fault of the 2024 Mw4.8 New Jersey earthquake which occurred near the misoriented 300-km long Ramapo Fault, by integrating seismicity-guided field geological mapping with friction experiments and slip tendency analysis. We find that the up-dip projection of relocated aftershocks aligns with a zone of NNE-striking topographic (LiDAR) traces of fault scarps, marking a previously unmapped fault zone in the New Jersey Highlands, henceforth designated as “Mountainville Fault (MF).” In basement outcrops along the topographic lineaments, we observe a predominance of NNE-striking/E-dipping, slickensided, gougeless fracture clusters with horsetail tip-splays, indicating a brittle shear zone origin. The fractures are poorly coalesced, and comprise steeply-dipping sets that are crosscut by gently-dipping sets. At the surface, MF lacks a break-through principal slip surface (core), and the geomorphic scarps and fractures strike at ∼15–25° obliquity to the mainshock's nodal plane, suggesting that the field-mapped structures represent the Riedel-shears of a deeper blind fault core, characteristic of an “immature” fault zone. Laboratory-constrained frictional behavior of sampled representative fault rocks, and slip tendency computation from focal mechanism-resolved stress field predict frictional instability of the MF. Additionally, the friction experiment results suggest a possible contribution of concealed fluid-rock alterations at the depth of the mainshock. Altogether, these MF characteristics fit those of other structurally investigated earthquake sources in the region, demonstrating the seismic hazard of elusive, critically-oriented immature intraplate faults.

Plain Language Summary Studies of intraplate earthquake hazards commonly focus on mature, prominent faults. Yet, earthquake records document moderate-magnitude earthquakes on inconspicuous faults. The 2024 Mw4.8 Tewksbury, New Jersey earthquake occurred near the ∼300-km long Ramapo Fault, which, although constituting the largest regional fault, is misoriented for slip in the current tectonic stress regime. The upward projection of aftershocks aligns with the topographic (LiDAR) trace of a previously unmapped fault zone 3.5 km west of the epicenter. We follow this lineament in the field, and all the examined bedrock exposures show clusters of subparallel, gougeless, paleo-slip surfaces with steeply-dipping sets crosscut by gently-dipping sets. Relative to the strike of the mainshock's nodal plane, the fractures and LiDAR fault scarps define Riedel-shears within a fault damage zone that lacks a breakthrough principal slip zone at the surface, characteristic of immature faults. We henceforth designate this fault as the “Mountainville Fault.” Laboratory friction experiments on sampled fault rocks predict earthquake occurrence mostly at the aftershock depth-range, suggesting possible concealed fluid-rock alteration phases at the relatively-shallower mainshock hypocenter. These structural characteristics fit previously investigated earthquake sources in the region, suggesting that immature basement faults may constitute important seismic hazards in intraplate settings than previously thought.

1. Introduction

In plate interiors, low tectonic strain rates inhibit accrual of elastic strain on pre-existing faults. Yet historical records document damaging earthquake ruptures on intraplate faults (e.g., Sykes, 1978; Sykes et al., 2008), suggesting that intraplate earthquakes are driven by transient processes that perturb the in situ stress field or fault strength (Calais et al., 2016). These observations also indicate that intraplate seismogenesis does not follow the “classical” tectonic seismic cycle. The lithosphere of the North American continent is pre-stressed, largely due to

Software: F. Kolawole, J. Tielke, C. McCarthy
Supervision: F. Kolawole, C. McCarthy
Validation: F. Kolawole, L. Seeber, W. Y. Kim, C. McCarthy, F. Waldhauser
Visualization: F. Kolawole, E. Beaucé, M. Colet, J. Tielke, A. Prakash, R. Ajala
Writing – original draft: F. Kolawole, E. Beaucé, Z. Foster-Baril, M. Colet, C. McCarthy
Writing – review & editing: F. Kolawole, E. Beaucé, M. Colet, L. Seeber, J. Tielke, A. Prakash, W. Y. Kim, R. Ajala, F. Waldhauser

the combined effects of far-field "ridge-push" tectonic stresses of the Mid-Atlantic Ridge (e.g., Zoback & Zoback, 1989) and long-term stress changes from post-glacial lithospheric rebound from the last ice age (e.g., Craig et al., 2023). Thus, the interseismic period of basement-rooting intraplate faults could become shortened by small-magnitude local perturbations to their stress state, commonly via increase in pore pressure or poroelastic effects from subsurface fluid injection or withdrawal (e.g., Ellsworth, 2013; Foulger et al., 2018; McGarr et al., 2015), surface water loading or unloading in dams (e.g., Gupta, 1992; Seeber et al., 1996), mining-related rock removal, and quarry unloading (e.g., Hasegawa et al., 1989; Seeber et al., 1998). Seismic hazard assessments of intraplate regions commonly focus on the larger, more mature fault systems due to their large surfaces that can host moderate-to-large earthquake events (e.g., Crone & Wheeler, 2000; Rimando & Peace, 2021; Wheeler & Crone, 2001). Yet, these regions commonly host energetic strain release on less-prominent frictionally-unstable basement-rooted faults (e.g., Kolawole et al., 2019), highlighting a possible fundamental difference in the relationships between fault structure and the nature of strain release in intraplate settings versus high strain-rate environments.

The 5 April 2024 Mw4.8 Tewksbury, New Jersey Earthquake (Figures 1a–1c) ruptured a previously unmapped basement-hosted fault with a hypocentral plane that strikes $013 \pm 0.9°$ (dips $45 \pm 4°$), at high angle to the ∼300-km long ENE-to-NE-striking Ramapo Fault, the largest mapped fault in the region (Figures 1b and 1c, Figures S1, S2a, and S2d in Supporting Information S1; Han et al., 2024; Boyd et al., 2024; Beaucé et al., 2025). The event nucleated at ∼4 km depth in the crystalline footwall of the Ramapo Fault (Figure 1c) with a slip area of 1.1 km radius (Han et al., 2024). Although, the earthquake was an oblique dextral thrust event (Figure 1b), the previously recorded events in the region are mostly thrust faulting (Figure 1b), documenting a compressive stress regime with ENE-WSW-to-NE-SW-oriented maximum compressive stress (SHmax) axis (Figure 1b). Thus, the Ramapo Fault and its sub-parallel neighboring faults are misoriented for reactivation in the current stress state, highlighting the need to understand the structure and geomechanical characteristics of secondary basement-hosted brittle faults in the region.

The epicenter region of the Mw4.8 event only experienced minor surface damage (small rockfall and wall collapse; Figures 1d–1f) consistent with a blind fault rupture (Figures 2a and 2b; Han et al., 2024). Preliminary analysis suggests that the low seismic attenuation of the regional crust and a downward rupture propagation (Han et al., 2024) make the event one of the widest-felt earthquakes in US history. Furthermore, it is one of the largest earthquakes in the Greater New York region since the 1884 Mw5.3 New York City earthquake and adds to the growing number of Mw < 5 events in the area, most of which are <15 km into the footwall of the Ramapo Fault System (Figure 1b). Here, we explore the causative fault of the 2024 Mw4.8 New Jersey Earthquake and investigate its geological and mechanical characteristics. By evaluating our findings with regard to the previously studied seismic sources in the region, we elucidate on the critical roles of fault zone structure on intraplate seismogenesis.

1.1. The Intraplate Seismicity and Geology of the Greater New York Region

In the Greater New York region, the hypocenters of most historical earthquakes are <10-km deep and occur within the Proterozoic-Paleozoic crystalline basement (Sykes et al., 2008). Notable seismic events include the 2024 Mw1.7 Astoria, 1985 Mw4.0 Ardsley, and the 1884 M5.3 NYC earthquakes (CBS News, 2024; Sykes et al., 2008). Although the mapping of active faults in the region is minimal, the previously studied seismic sources include the Dobbs Ferry Fault (Dawers & Seeber, 1991) and the 125th Street Fault (CBS News, 2024; Sykes et al., 2008). The fault responsible for the 1884 M5.3 NYC Earthquake, the largest event in the region, remains unknown (Sykes et al., 2008).

The Ramapo Fault System is the border fault of the Mesozoic Newark Rift basin, juxtaposing Grenvillian (Mesoproterozoic) metamorphic rocks in its footwall (northwest) against Triassic-Jurassic volcano-sedimentary syn-rift sequences in its hanging wall to the southeast (Figures 1b and 1c, Figures S2a and S2e in Supporting Information S1; Ratcliffe, 1971; Ratcliffe et al., 1986; Withjack et al., 2013). The Grenville terrane hosts moderately foliated hornblende granites, quartz-oligoclase foliated gneisses, and diorites of the Bryram intrusive and Losee metamorphic suites (Drake, 1984; Rankin et al., 1989; Drake et al., 1991; Figure S1 in Supporting Information S1). In the Tewksbury area, geologic maps label the border fault as "Clinton Fault' (Figure S1 in Supporting Information S1; Volkert, 2021); in this contribution, for regional consistency, we refer to the basin-bounding fault as the "Ramapo border fault system."

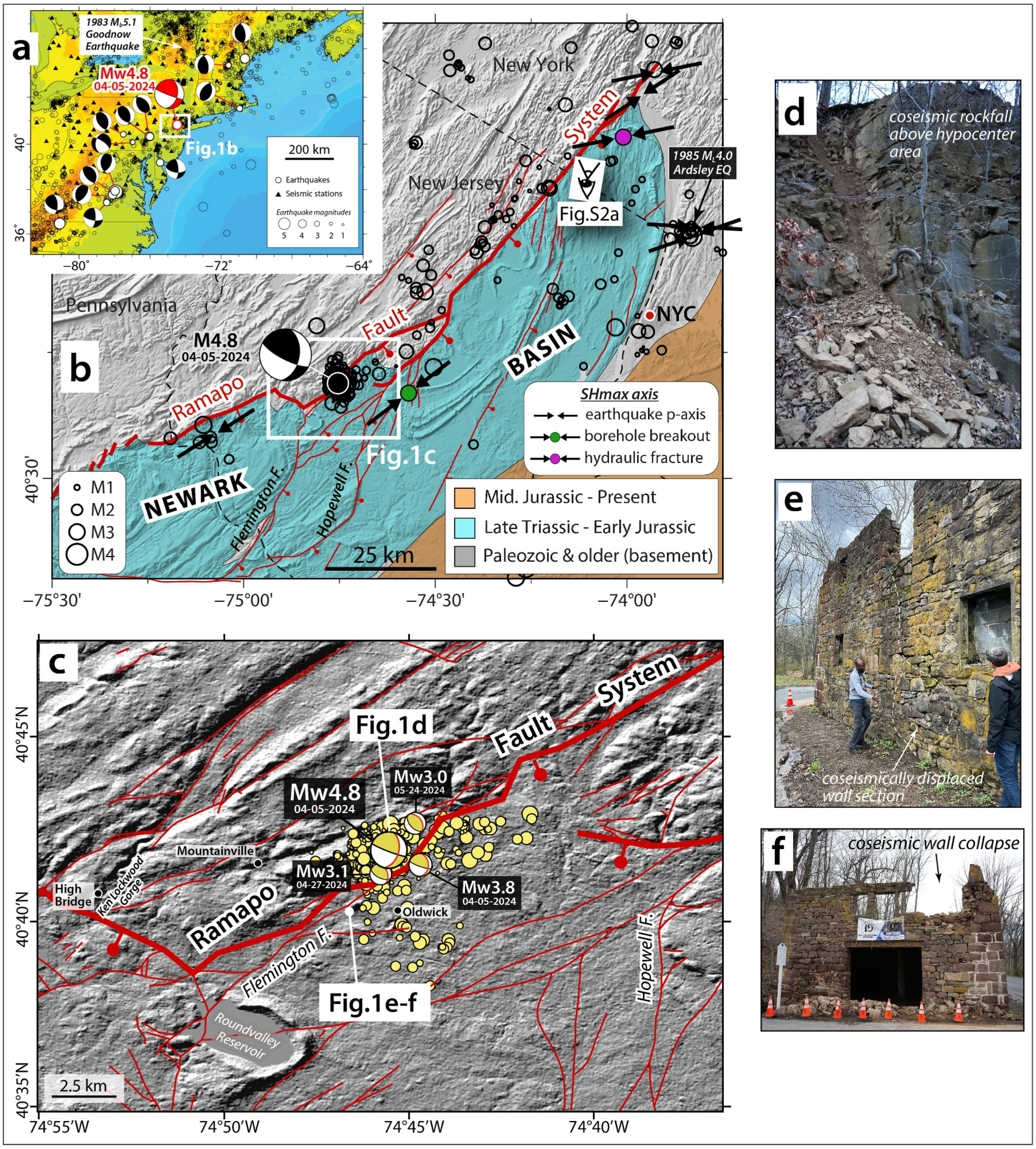

Figure 1. (a) Eastern-North America's historical seismicity since 1990 (Table S1 in Supporting Information S1; Source: USGS earthquake catalog; Du et al., 2003; Kim & Chapman, 2005; Sykes et al., 2008; Han et al., 2024). (b) Generalized geologic map of the Newark Basin (after Withjack et al., 2013) showing seismicity and SHmax axes (Goldberg et al., 2003; Sykes et al., 2008). (c) 3-m LiDAR topographic relief map of Tewksbury, New Jersey (source: USGS) showing aftershocks of the 2024 Mw4.8 event (yellow circles; Beaucé et al., 2025) and previously mapped faults (from New Jersey Geological and Water Survey fault database). (d–f) Observations of minor coseismic surface deformation at the hypocenter and at distance away suggesting a blind, but shallow fault rupture.

2. Data and Methods

2.1. Field Mapping of Brittle Deformation Across Tewksbury, New Jersey

High-resolution locations of aftershocks (Figures 2a and 2b, Beaucé et al., 2025) resolve the broad subsurface geometry of the causative fault zone; however, they lack the meter-scale details of the geological and geomechanical characteristics of the fault. To delineate the surface continuation of the causative fault zone, we integrate the up-dip projection of the relocated aftershocks with shaded relief maps of available Light Detection and Ranging data (LiDAR) digital elevation models (DEM) covering the Tewksbury region to support geological

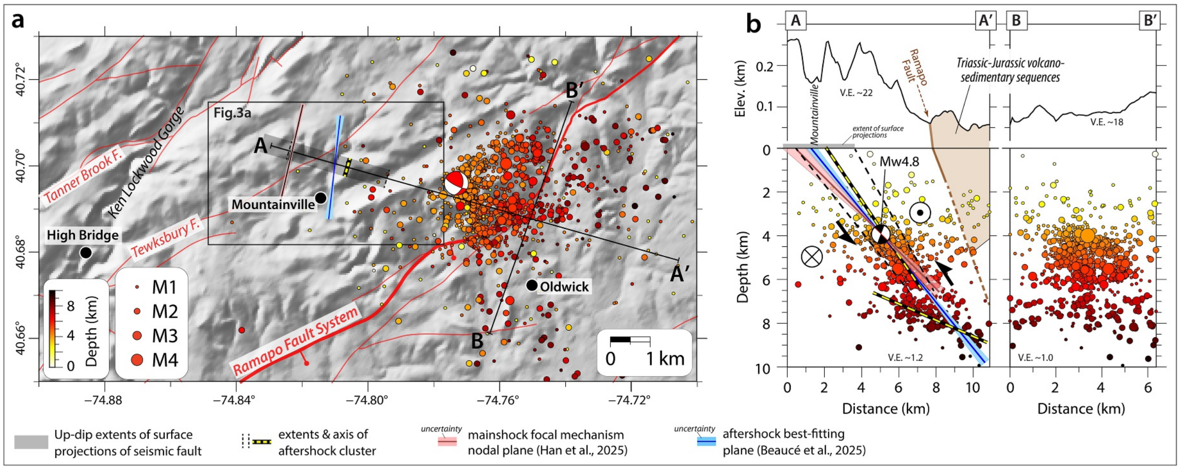

Figure 2. (a) Shaded relief map of Tewksbury region overlaid with relocated aftershocks from Beaucé et al. (2025) and (b) Cross-sectional profile of the aftershocks with up-dip surface projections of the ESE-dipping seismic fault, including focal mechanism nodal plane (Han et al., 2024; strike: 013 ± 0.9°, dip: 45 ± 4°ESE) and aftershock best-fitting plane (Beaucé et al., 2025; strike: 006.4 ± 4.4°, dip: 51 ± 2°ESE). The aftershocks delineate at least two distinct segments of the ruptured fault zone (dashed black/yellow lines). Altogether, the resolved seismic fault zone projects up-dip to Mountainville area.

field mapping efforts. We utilize 3-m LiDAR DEM (NJ HUNTERDON 2006) and 0.6-m Bare Earth LiDAR DEM (NJ NW6Co 2017), available through the geospatial database of the United States Geological Survey (USGS). Due to the density of vegetation in the study area, the 3-m LiDAR data only resolve the most prominent topographic lineaments in the landscape, whereas the 0.6-m bare earth LiDAR data has significantly higher resolution to resolve fault scarps on the landscape that are hidden by vegetation. Delineated steep scarps within the area of surface projection of the aftershock cluster provide important geomorphic evidence that may hint at potential Quaternary fault activity in the area. In the field, we map the brittle deformation patterns in the bedrock exposures across the region. Previous studies in intraplate seismic zones in Central US show that active basement-rooted faults continue up to the Top-basement unconformity, and that the fault-fracture systems are mappable on the basement surface where accessible, either in outcrops (e.g., Kolawole et al., 2019, 2026) or in geophysical images of buried basement (Chase et al., 2023; Firkins et al., 2020; Kolawole et al., 2020; Magnani et al., 2017; Patel et al., 2021). In Tewksbury, we extend our field mapping outward from the location of up-dip projection of the seismicity clusters, into the surrounding areas to characterize the deformation and constrain the most probable surface location of the causative fault zone. A limitation of this approach is spatially discontinuous and sparse outcrops, which are common to bedrock geological mapping in the east coast and similar settings where vegetation and built-up townships are extensive.

2.2. Frictional Stability Testing of Representative Fault Rock Samples

In the elasto-frictional regime of the brittle crust, seismogenic strain release on Coulomb-optimal slip surfaces depends on the frictional stability of the fault rocks. Given an effective stress loading condition in the subsurface, the frictional stability behavior of fault rocks is strongly controlled by the lithological composition and temperature (e.g., Blanpied et al., 1998; Ikari et al., 2011; Kolawole et al., 2019). To better understand the subsurface conditions of unstable failure around the hypocentral zone of the 2024 New Jersey earthquake, and to delineate the representative frictional strength of the earthquake-hosting fault rocks in the region, we perform standard friction experiments on two representative fault rock samples from the study region: (a) Hypersthene-quartz-plagioclase gneiss from Mountainville area of Tewksbury (location in Figure S1 in Supporting Information S1), and (b) brecciated Hornblende granite gneiss from an exposure of the Ramapo Fault in Suffern (Figure S2 in Supporting Information S1). Hornblende granite gneisses are generally ubiquitous in the Grenvillian age terranes along the footwall of the Ramapo Border fault system and also dominate the basement in the Tewksbury Township area (Figure S1 in Supporting Information S1).

For our friction experiments, we use a NER Autolab 2000 triaxial deformation apparatus (Figures S3a and S3b in Supporting Information S1) and the detailed experimental set up and procedure are provided in Text S1 in Supporting Information S1. In the apparatus, shear deformation was applied to the gouge in a series of velocity steps ranging from 0.3 to 30 μm/s, in logarithmic increments, up to a maximum displacement of 5 mm. The friction coefficient ($\mu = \tau/\sigma_n$) was calculated by taking the shear stress τ as the axial force divided by the shear area, and the normal stress σ_n as the confining pressure. Data from calibrated pressure transducers, the internal load cell, and an external linear variable differential transformer were recorded at 10 Hz. The Matlab-GUI RSFit3000 described in Skarbek and Savage (2019) was used to process raw velocity steps to determine key parameters, including the frictional stability ($a - b$) shown in the main text. The GUI uses Equation 1 the empirical rate-and-state friction law:

$$\mu = \tau/\sigma_n = \mu_0 + a \ln(\mathrm{V}/\mathrm{V}_0) + b \ln(\mathrm{V}_0\Theta/\mathrm{Dc}) \tag{1}$$

in which a is the "direct effect" due to a change in slip velocity from a reference velocity V_0, b is the "evolution effect," and Dc is the critical slip distance needed for the system to evolve from one steady-state to the next (Dieterich, 1979; Marone, 1988; Rice & Ruina, 1983), Equation 2 both the aging- (Dieterich, 1978) and slip- (Ruina, 1983) forms of state evolution, although here we report results from the aging law:

$$\mathrm{d}\Theta/\mathrm{d}t = 1 - \mathrm{V}\Theta/\mathrm{Dc} \tag{2}$$

and Equation 3 Hooke's law applied to a single-degree-of-freedom spring slider to approximate the elastic response of the apparatus and sample:

$$\mathrm{d}\mu/\mathrm{d}t = k(\mathrm{VL} - \mathrm{V}) \tag{3}$$

in which inertia is negligible, and the frictional surface is assumed rigid so that all elastic deformation is included in k, the spring constant of the loading environment. The GUI casts S1, S2, and S3 as coupled ordinary differential equations and, here with a single slip variable, uses a nonlinear least squares fit to minimize the difference between the data and μ, a, b, and Dc user inputs. The relative values of a and b from this treatment describe the frictional stability of the system at each step in velocity. We describe the method for analyzing the composition of the tested gouges in Text S2 in Supporting Information S1.

2.3. Focal Mechanism-Based Stress Inversion and Reactivation Tendency Calculations

2.3.1. Focal Mechanism-Based Stress Inversion

We perform a regional stress inversion using earthquake focal mechanisms near the Tewksbury area, between 39.20°N to 41.00°N and −76.06°E to 74.00°E, following the approach of Vavryčuk (2014). We use the already available mainshock and three aftershock focal mechanism solutions for the 2024 Tewksbury earthquake (Han et al., 2024) as well as eight regional focal mechanisms across the Newark Basin (Table S2 in Supporting Information S1; Kim et al., 2026) to help constrain the inversion. The stress inversion methodology is based upon the linear inverse problem relating focal mechanisms with the Cauchy stress tensor (Michael, 1984), based on the assumption that slip occurred along the direction of maximum shear stress (Wallace-Bott assumption) and that all faults broke at the same shear stress level. Out of the two nodal planes provided by each focal mechanism, the algorithm picks the most likely set of fault planes using the Mohr-Coulomb failure criterion (Vavryčuk, 2014). We use the open-source ILSI program (Iterative Linear Stress Inversion; Beaucé et al., 2022; see Open Research section), which employs a Bayesian solution (Tarantola & Valette, 1982) and estimates uncertainties by bootstrapping the focal mechanisms and repeating the inversion. To quantify the relative stress magnitudes, we use the definition of the shape ratio $R = (\sigma_1 - \sigma_2)/(\sigma_1 - \sigma_3)$. Given the relatively small set of the focal mechanism data set, we used the prior Bayesian constraint that one principal stress is near vertical to regularize the inversion. Further, to assess the validity of our solution, we calculate the mean angle (β) between the predicted resolved shear stresses and observed slip directions (after Michael, 1984).

2.3.2. Analysis of Fault Reactivation Tendency Using the Resolved Tectonic Stress

To assess the relationship between the Mountainville Fault zone and the 2024 Mw4.8 event, we examine the slip tendency of the mapped paleo-slip surfaces in the resolved contemporary stress field of the Tewksbury area. We adopt the method of Vavryčuk (2014) and Beaucé et al. (2022) in which reactivation slip tendency is calculated

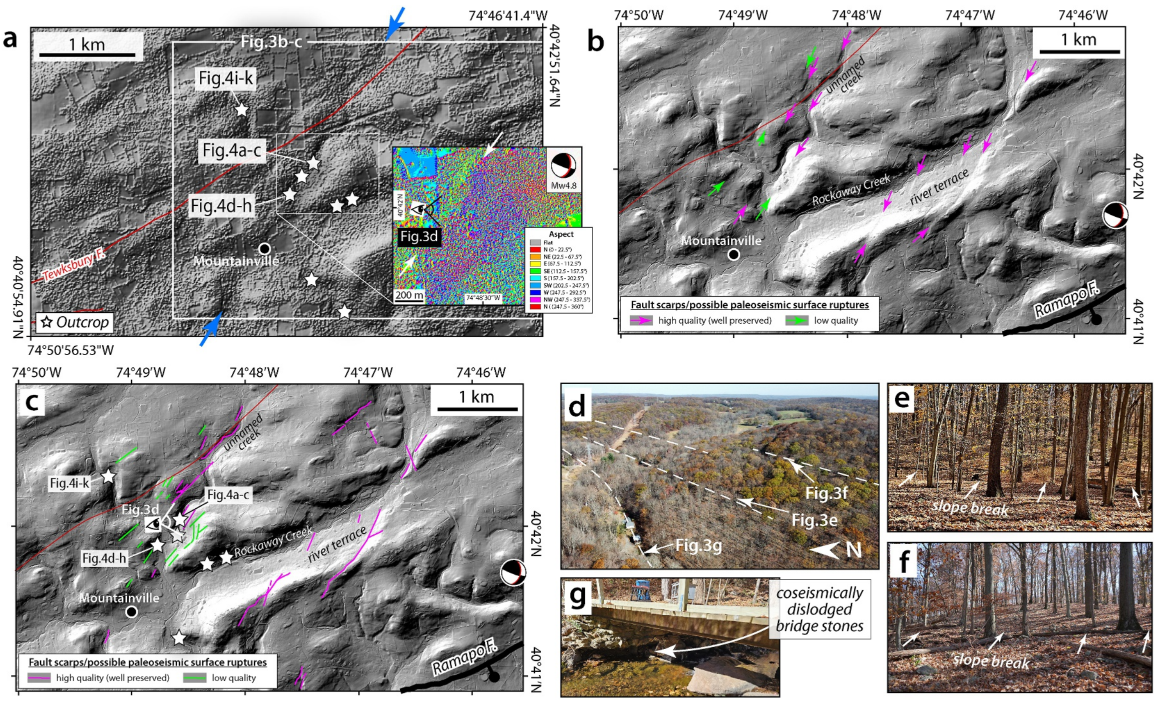

Figure 3. (a) 3-m LiDAR relief map of the Mountainville area revealing a prominent NNE-striking geomorphic lineament in Mountainville area that is oblique to- and crosscuts the previously mapped Tewksbury Fault. Inset: Aspect map of the LiDAR data revealing NNE-striking slope break marking the base of an escarpment along the trace. (b, c) Bare earth 0.6-m LiDAR relief map of Tewksbury area revealing NNE-striking rectilinear fault scarps in Mountainville area and east of the area (between Mountainville and the Mw4.8 epicenter). (d) A landscape photograph taken with an unmanned aerial vehicle, and (e, f) field photographs of NNE-striking slope-breaks on the broad NW-facing elevated escarpment along the LiDAR lineament. (g) Coseismically-displaced stone footing of a bridge reported by the property owner.

via the "fault instability parameter" but shares similarities with the standard slip tendency parameter of Morris et al. (1996). We use stress tensors obtained from the inversion of the earthquakes to examine their likelihood to reactivate the mapped fault-fracture systems in the exposures of the Mountainville Fault Zone, and in the regions to the east and west of the Mountainville area. For the analysis, we include the nodal planes of the mainshock and aftershock focal mechanisms in order to further validate the test. Although this analysis assumes a cohesionless fault, and that fault strength comes primarily from friction between the gouge particles (Figure 6a), we acknowledge that the intraplate nature of the setting implies there might be long-term fault healing and elevated fault rock cohesion. However, a quantitative investigation of fault rock cohesion is beyond the scope of the current study.

3. Results

3.1. The 2024 M4.8 Tewksbury Earthquake Causative Fault

3.1.1. Aftershock and Topographic Delineation of the Causative Fault

In the relocated aftershock catalog, the broad three-dimensional (3-D) geometry of the seismicity cluster defines a ESE-dipping primary structure with two segments consisting of a shallow steeper segment (~59° dip), and a deeper lower-angle segment (~24° dip) (see A–A′ in Figure 2b). However, hypocenter density plots by Beaucé et al. (2025) delineate a NNE-SSW (006.4 ± 4.4°)-striking, 51 ± 2.0° ESE-dipping slip zone. The range of dips of the aftershock cluster is consistent with 45° dip of the Mw3.8 aftershock nodal (Figure 1c), but may reflect a variability in the dip of slip surfaces are depth. The epicenters are mostly confined to the exhumed Proterozoic basement footwall of the Ramapo Fault (Figures 2a and 2b). Up-dip projections of the relocated aftershocks, mainshock nodal plane (Han et al., 2024), and aftershock best-fitting plane (Beaucé et al., 2025) and their uncertainty halos point to the Mountainville area of Tewksbury (Figures 2a and 2b). The surface projections are co-located with a NNE-striking topographic lineament in the 3-m resolution LiDAR data (see shaded relief map in Figure 3a). The lineament is oblique to- and crosscuts the previously mapped Tewksbury Fault that strikes ENE-

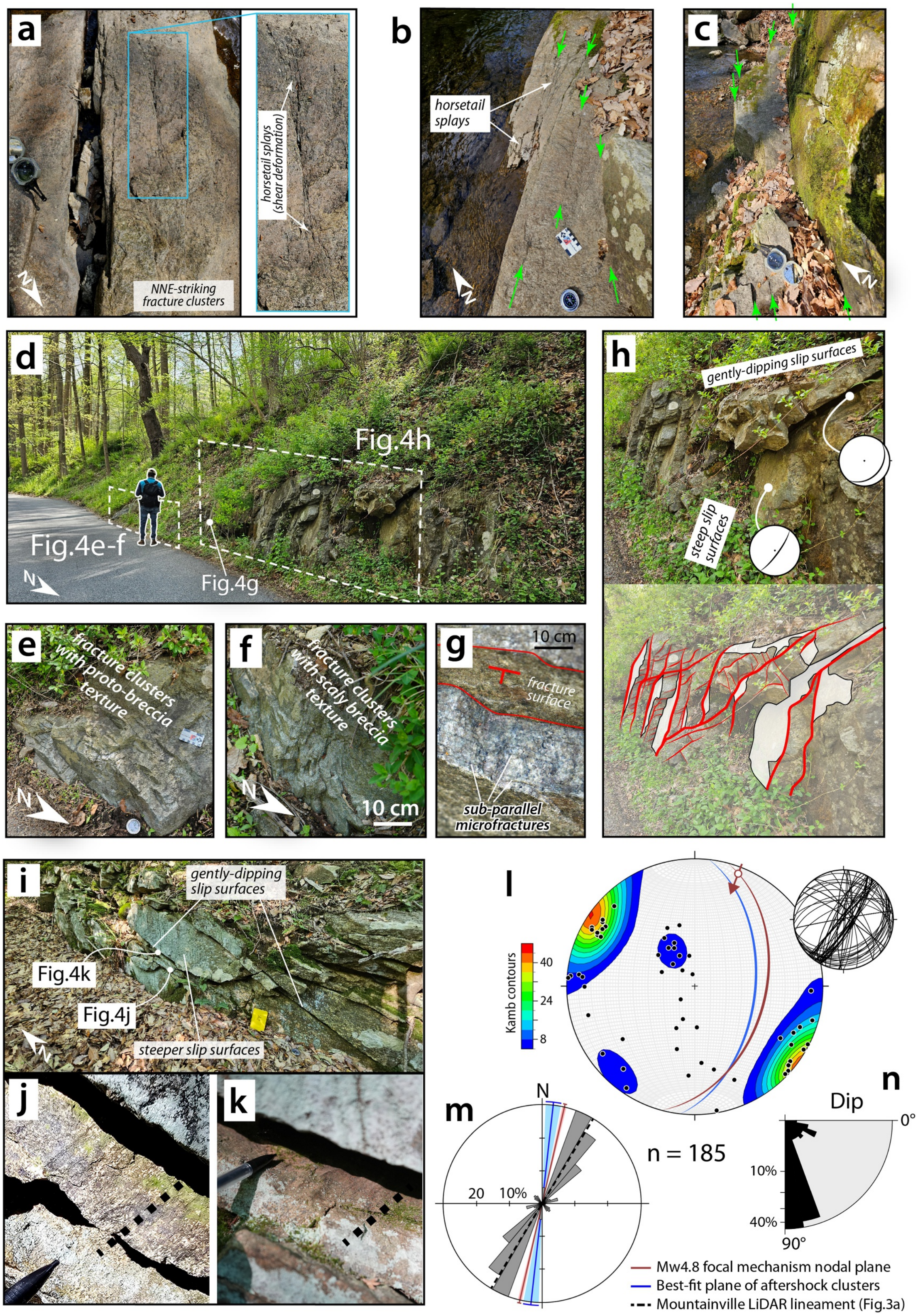

a
horsetail splays (shear deformation)
NNE-striking fracture clusters
N
b
horsetail splays
N
c
N
d
Fig.4h
Fig.4e-f
Fig.4g
N
h
gently-dipping slip surfaces
steep slip surfaces
e
fracture clusters with proto-breccia texture
N
f
fracture clusters with scaly breccia texture
N
10 cm
g
10 cm
fracture surface
sub-parallel microfractures
i
gently-dipping slip surfaces
Fig.4k
Fig.4j
steeper slip surfaces
N
j
k
l
Kamb contours
40
24
8
m
N
20
10%
n = 185
n
Dip
0°
10%
40%
90°
Mw4.8 focal mechanism nodal plane
Best-fit plane of aftershock clusters
Mountainville LiDAR lineament (Fig.3a)

Figure 4.

to-NE north of Mountainville (Figure 3a), oriented parallel to the larger Ramapo Fault (see Figure 2a). This lineament, which continues southwest across the Mountainville, defines a strong topographic gradient that bounds a WNW-facing escarpment (white arrow in Figure 3a inset) and strikes obliquely (~15°) to the mainshock nodal plane (Figure 3a inset). The higher resolution (0.6-m) bare earth LiDAR relief map of Tewksbury (Figures 3b and 3c) reveals the presence of NNE-striking <1.5 km long fault scarps on the Quaternary post-glacial landscape, most of which appear to cluster along the delineated topographic lineament in the 3-m LiDAR map. Some of the scarps crosscut both the gneissic bedrock ridges and adjacent Quaternary river terrace sediments (Figures 3b and 3c). The escarpments bounding the trace of the 3-m LiDAR topographic lineament host rectilinear slope breaks (Figures 3d–3f) that strike parallel to the LiDAR lineament (Figure 3a inset, Figure 3c). Here, a local property owner reported that bridge stone footings were coseismically dislodged during the 5 April 2024 Mw4.8 event (Figure 3g). In the field, we follow this prominent topographic lineament along-strike and map the brittle deformation patterns in bedrock exposures. To better constrain the surface location of the causative fault zone, we extend the mapping eastward (across the epicenter area, north of Oldwick) and westward (to High Bridge and Ken Lockwood Gorge areas) (Figure 2a).

3.1.2. Basement-Hosted Fault-Fracture Systems in Tewksbury

Published geologic maps of the Tewksbury region show a predominance of ENE-to-NE striking faults in the Ramapo Fault footwall, including the Tanner Brooke and Tewksbury faults (Figures 1b and 1c, Figure S1 in Supporting Information S1), presupposing that the brittle deformation of the basement is defined by faults that are parallel to the Ramapo Fault. However, since the aftershocks define a NNE-striking causative fault, the brittle damage of the causative fault must define a fault zone that strikes at a high angle to the Ramapo Fault. In Tewksbury, the basement is composed of hornblende granite gneiss with in-folded diorite gneiss and hypersthene-quartz-plagioclase gneiss (Figure S1 in Supporting Information S1; Volkert, 2021).

At all the accessible bedrock exposures along the trace of the LiDAR lineament, we find widespread brittle deformation that is characterized by sub-parallel fractures that commonly occur in clusters (Figures 4a–4h), and in many places, exhibit horsetail splays at their tips (Figures 4a–4c). Down-dip, the fracture sets show cross-cutting sets of two dominant dip sets defined by a steep set that is crosscut by a gently-dipping (~30°) set (Figures 4d, 4h, 4i–4k). Nevertheless, at one of the exposures, we note that one of the steep slip surfaces appears to have coalesced with a lower-angle surface up-dip, defining a continuous slip surface (Figure 4h). Sections of the fracture clusters exhibit scaly breccia textures (Figures 4e and 4f, Figures S4a and S4b in Supporting Information S1). In general, the fractures are commonly hematite-altered and slickensided or polished, but commonly lack slickenlines and gouge development, indicating low displacement paleo-slip surfaces (Figures 4g and 4h). We plot all the fracture measurements taken in outcrops along the LiDAR lineament showing that the structure is dominated by NNE-SSW-striking (020°–030° peak azimuth) fractures (Figures 4l and 4m), and although NW-dipping sets exist, the majority of the fractures are ESE-dipping (Figure 4l). Our plot of dip angles of the fractures supports the observations of two distinct dip sets of steep and gently dipping planes (see frequency-dip distribution in Figure 4n). Overall, we do not find a breakthrough principal fault that connect these fracture clusters, and the fractures dominantly strike at ~15° obliquity to the main nodal plane of the mainshock event (red line, Figure 4m) and at ~22° obliquity to the best-fit plane of aftershock clusters (blue line, Figure 4m).

To the east and west of the Mountainville area, the fracture systems and their field relationships contrast with those of the MF. In areas surrounding the mainshock epicenter where bedrock outcrops record minor coseismic rockfall (Figure 1d), we observe relatively sparse basement fracturing with a bi-modal distribution of ENE-striking (i.e., Ramapo Fault-parallel) and NW-to-NNW-striking fractures, which also exhibit hematite

Figure 4. (a–f) Photographs of observed pre-existing brittle deformation in Precambrian gneissic outcrops along the LiDAR fault trace, showing predominance of sets of NNE-striking, ESE-dipping fracture clusters, but lack a breakthrough principal slip zone. The common presence of fracture tip horsetail splays (panels a–c), and protocataclastic textures (panels e–f, also Figures S4a and S4b in Supporting Information S1) suggest a deformational origin of brittle shear. (g) Zoomed-in photograph showing that even at micro-scale, the deformation is characterized by sub-parallel hematite-altered fracture clusters. (h) An example of characteristic deformation relationships observed in outcrops where the 3-dimensional view of the fracture clusters can be seen, showing that although the fractures are sub-parallel, they can be sub-classified into two distinct dip sets (see global plot in panel n). (i–k) Outcrops at ~1 km west of the main LiDAR fault trace, presumably part of the fault zone, also showing intersecting sets of gentle-dipping and steep paleo-slip surfaces with oblique-thrust slip vectors. (l) Stereographic projections, (m) Frequency-azimuth plot, and (n) frequency-dip distribution of the fracture systems and slip planes mapped in outcrops along the fault zone. In panel (n), we overlay the mainshock nodal plane (from Han et al., 2024) and aftershock best-fit plane (from Beaucé et al., 2025) with their uncertainties (light pink and light blue).

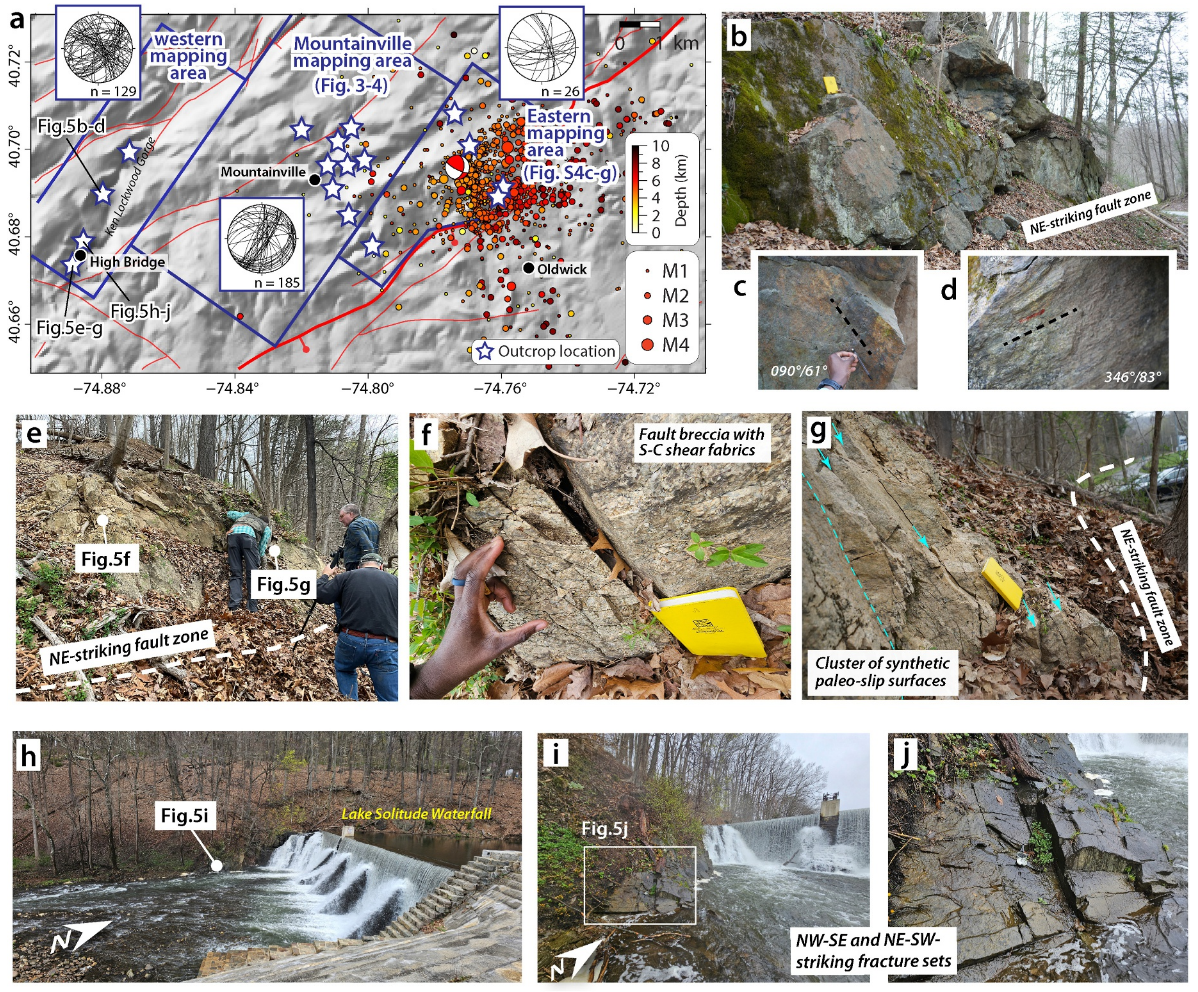

Figure 5. (a) Topographic relief map of Tewksbury area (same as in Figure 2a) showing the locations of outcrops and fault mapping in the areas west of Mountainville (i.e., High Bridge and Ken-Lockwood Gorge areas). Also included are outcrop locations in Mointainville area and the eastern mapping area with stereographic projections of the outcrop fracture populations mapped in each area. (b–d) Field photographs of a NE-SW -striking, SE-dipping fault zone with NE- and NW-striking slip planes and variable paleo-slip directions (oblique-thrust, panel c, and strike-slip, panel d). The fault locally controls the geometry of the Raritan River. (e–g) Field photographs of the exposed section of a NE-striking, SE-dipping fault zone in the town of High Bridge, exposed in an outcrop along Washington Avenue, by Union Forge Park; and (h–j) brittle damage zones with NE and NW-striking fracture sets in outcrops along the shore of Lake Solitude and its waterfall.

alterations and paleo-slip features (Figures S4c–S4g in Supporting Information S1; stereoplot inset in Figure S4c in Supporting Information S1). To the west of Mountainville (western mapping area, Figure 5a), we find the best bedrock exposures along the Raritan River, where the river flows south along a NNE-trending bedrock canyon (Figures 5a–5j). Field mapping in the western mapping area shows a predominance of NE-SW and NNW-SSE-striking fracture systems that are associated with NE-striking fault zones (Figures 5b–5g). Examples include a NE-striking fault zone hosts many slip planes with excellent preservation of slickenlines in the northern Ken Lockwood Gorge Bridge (Figures 5b–5d). Also, in High Bridge, a prominent NE-striking fault zone exhibits excellent S-C fabrics in incohesive brecciated gneisses (Figures 5e and 5f).

3.2. Frictional Behavior of Host Basement Fault Rocks

The results of frictional stability tests (Figures 6a and 6b) are typically presented by the friction rate parameter $(a - b)$ of the rate- and state-friction equation (Equation 1). If negative, the $(a - b)$ values indicate a velocity weakening behavior, consistent with favorable conditions for earthquake nucleation by the associated sample in that specific loading condition. Positive $(a - b)$ values indicate velocity strengthening behavior which suggest that at the associated loading conditions, the sample is more likely to creep and unlikely to nucleate an earthquake. In

10.1029/2025JB033723

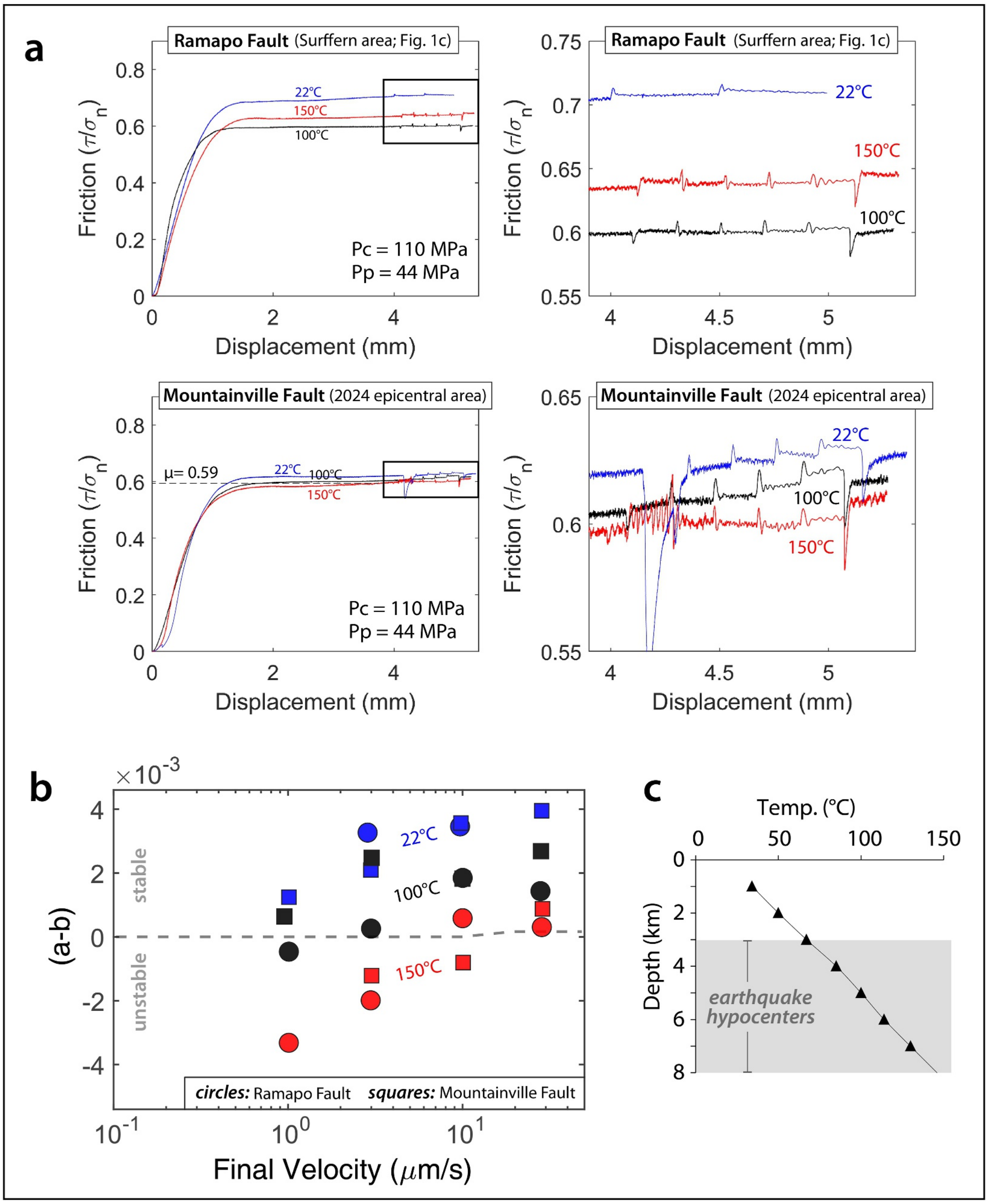

Figure 6. (a) Laboratory friction experiments and (b) resulting frictional stability plots for representative fault rocks in the area, comprising fault rock samples from the Ramapo Fault (Figures S2a–S2d in Supporting Information S1) and the Mountainville Fault Zone (Figure 4e). The Ramapo Fault sample is of hornblende granite gneiss protolith, and the Mountainville Fault of hypersthene-quartz-plagioclase gneiss protolith (Figures S1, S5a, and S5b in Supporting Information S1). Both samples exhibit ∼0.59 steady-state friction, and instability at >5 km (>100°C) depth conditions.

our study, friction tests reveal a stronger tendency for seismic instability at lower displacement rates for the two tested representative fault rock samples (Figure 6b). The fault rocks commonly show velocity strengthening behaviors at ≤5 km depth conditions (≤100°C), indicating a very low tendency to nucleate earthquakes at conditions relevant to those depths (Figures 6b and 6c). However, the samples transition to velocity weakening behaviors at 150°C and associated loading conditions, relevant to ∼8 km depth (Figures 6b and 6c). The Mw4.8 mainshock ruptured at ∼4.5 km depth (∼100°C), but the aftershocks are at greater depths (down to 9 km; Figure 2b). The fault rocks attain steady-state failure at $\mu = 0.59$–0.62 friction coefficient for the deeper loading conditions. Compositionally, both gouges host similar quartz concentrations and are generally dominated by

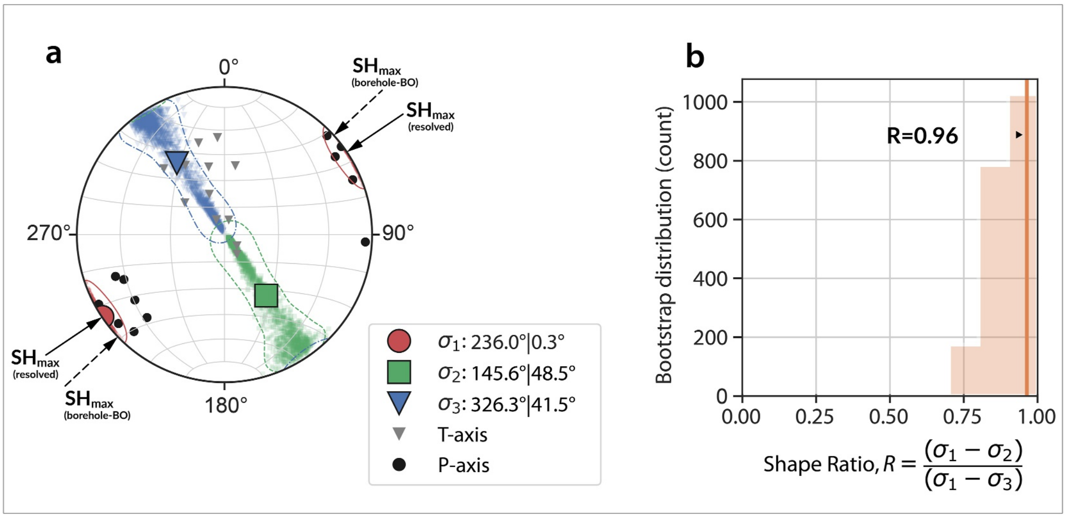

Figure 7. Stress tensor for the Newark Basin determined by 12 earthquake focal mechanisms located near the study area between 39.20°N and 41.00°N and 76.06°W–74.00°W (Table S2 in Supporting Information S1). (a) Resolved principal stress directions. Contours show the 95% confidence interval. Note that the 95% confidence interval of the SHmax trend is (223°–254°). Uncertainties were estimated with the bootstrap method. (b) Relative stress magnitudes (shape ratio) resolved from the focal mechanisms. Note that a shape ratio of $R = 0.96$ implies that $\sigma_2 \approx \sigma_3$.

feldspars, but with a single sodic phase dominating the Ramapo fault sample (70% albite), and a variety of phases characterizing the Mountainville fault sample (27.6% albite, 29.7% Oligoclase, and 21.1% microcline, with ∼13% Fe-rich hypersthene) (Figures S5a and S5b in Supporting Information S1).

3.3. Contemporary Slip Tendency of the Mapped Fault-Fracture Systems

Our inverted stress tensor (Figures 7a and 7b) reveals a transpressive stress regime with horizontal maximum compression (SHmax) trending NE-SW at 236° (with a range of 223°–254° at the 95% confidence interval) and $R = 0.96$. Uncertainties were computed by bootstrapping the focal mechanisms 2,000 times and we computed a mean angular misfit of $\beta = 15.2°$. The resolved SHmax orientation and confidence interval are consistent with the estimate from borehole breakout measurement near Tewksbury (Figures 1b; 227° SHmax trend at ∼1 km depth; Goldberg et al., 2003).

Using the resolved stress field and a friction coefficient (μ) of 0.59 from our fault rock friction experiments (Figure 6a), estimated slip tendencies provide insight into the stress states of the mapped fault-fracture systems. The results for the Mountainville Fault Zone are presented in Figures 8a and 8b, those for areas east of Mountainville (epicenter area, north of Oldwick) in Figures 8c and 8d, and areas west of Mountainville (Ken-Lockwood Gorge/High Bridge areas) in Figures 8e and 8f. Although the three areas host critically stressed fault planes, the Mountainville Fault Zone hosts the most predominant concentration of such planes (Figures 8; 62% of the planes show >0.9 slip tendency, compared to only 34.6% east and 23.3% west of Mountainville). In the Mountainville Fault Zone, the results show that show that only the NNE-striking, steep east-dipping slip surfaces are the most critically stressed, exhibiting similar slip tendency to the earthquake focal mechanism nodal planes (Figures 8a and 8b). The lower-angle NNE-striking planes in the fault zone exhibit much lower (0.6–0.7) slip tendencies. The slip tendency calculation for each of the 2000 bootstrap stress tensors shows that our results were robust to the extent of the uncertainties (see Figure 8g).

4. Discussions

4.1. The Structure and Origin of the Causative Fault Zone

The co-location of the Mountainville Fault with the surface projections of mainshock nodal planes and aftershock best-fitting planes (Figures 2a and 2b) suggest that the mapped NNE-striking brittle shear zone marked by LiDAR topographic scarps in Mountainville is the surface manifestation of the fault zone that hosted the 5 April 2024 Mw 4.8 Tewksbury earthquake event. Also, the high reactivation tendency of its slip surfaces in the resolved tectonic

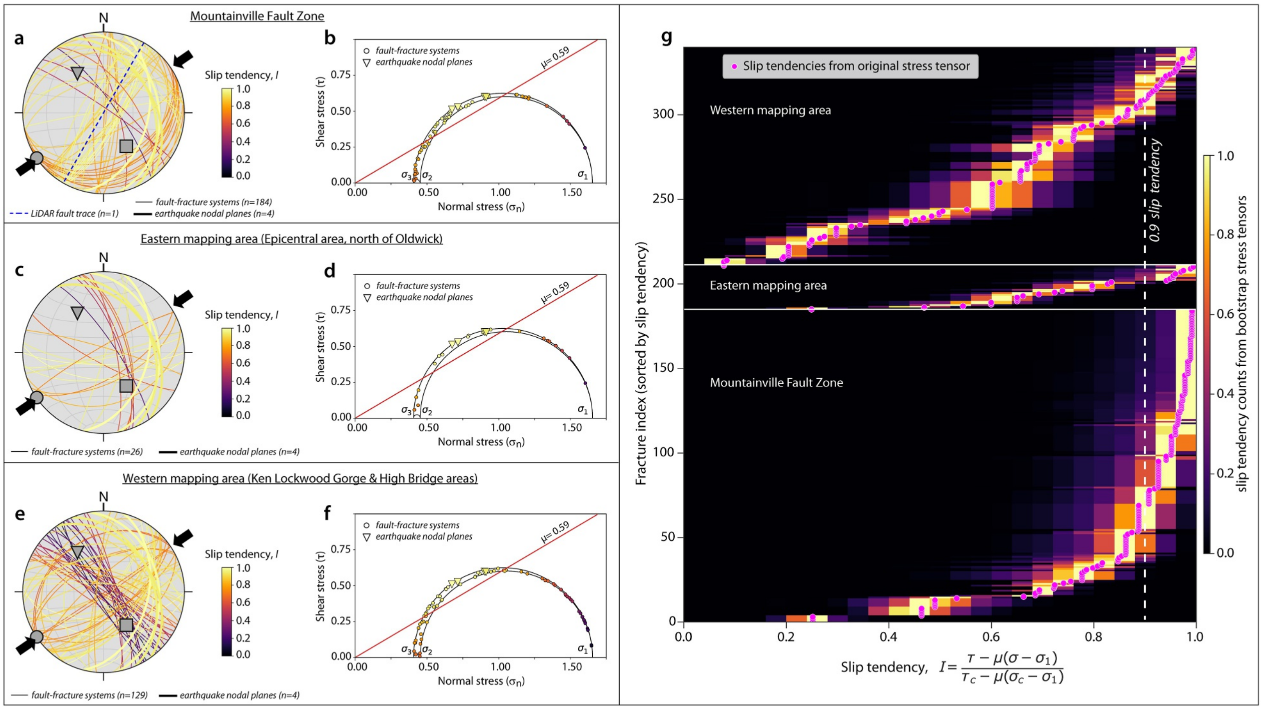

Figure 8. Plots showing slip tendency estimates for (a, b) the Mountainville fault-fracture systems, and (c–f) fault-fracture systems in the eastern and western mapping areas (see map in Figure 5a), using the resolved Newark Basin stress field (Figure 7) and the laboratory-derived friction coefficient of the representative fault rocks (Figure 6a). Slip tendency is defined as in Vavryčuk (2014) and Beaucé et al. (2022). (g) Uncertainties in slip tendency estimates propagated from the range of uncertainties in the regional stress inversion (see method section). Color shows the distribution of slip tendency for each fracture, to compare with the slip tendencies computed with the original stress tensor (magenta dots). σ_c and τ_c are critical normal stress and shear stress respectively, for which slip tendency = 1.00.

stress field suggests a causative relationship between the fault zone and the earthquake event given the significantly greater predominance of critically-stressed (>90% slip tendencies) slip planes in the fault zone compared to the surrounding areas (Figure 8g). The slip tendency results suggest that slip planes of steep and intermediate-dips in the fault zone are critically stressed in the modern stress field, similar to the 2024 earthquake nodal planes (Figures 8a and 8b). In the Tewksbury area, the fault scarps revealed by the 0.6-m LiDAR data (Figures 3b and 3c) appear to cut the broad Quaternary Laurentide- and pre-Laurentide glaciated surface of the New Jersey Highland/Reading Prong region. As of the time of this study, our field observations do not show any evidence of an 5 April 2024 coseismic surface rupture along the exposures of the fault zone, consistent with the 4 km mainshock hypocenter and the 1.1 km slip radius (Han et al., 2024).

The internal geological structure of the surface-mapped brittle shear zone suggests that the fault zone is an "immature" basement-hosted fault. We designated this fault zone as the "Mountainville Fault" (MF). Many studies of brittle faulting in basement outcrops (e.g., Blenkinsop, 2008; Faulkner et al., 2003; Faulkner et al., 2011; Gabrielsen & Braathen, 2014; Mitchell & Faulkner, 2009; Segall & Pollard, 1983) and experimental models of their evolution (e.g., Liao et al., 2017) show that at the initial stage of development where accrued displacement is very small, synthetic (R) shear fractures dominate a fault zone (Figure 9a). The studies show that with displacement accrual and maturity, a breakthrough principal slip surface subsequently emerges (p-shears), with the proximal segments of the R-shears (and antithetic R' Shears if present) merging with the principal fault core (Figure 9a). Irrespective of lithology, faults smoothen and slip surface networks coalesce with increasing displacement accrual and maturation (Brodsky et al., 2011; Sagy & Brodsky, 2009). In crystalline basement rocks, "immature" (low-offset) fault zones commonly exhibit pervasive clustering of slickensided fracture sets with little gouge accumulation (e.g., Gabrielsen & Braathen, 2014; Kolawole et al., 2019, 2026). In Tewksbury, our field observations reveal that the Mountainville Fault zone is dominated by sub-parallel arrays of slickensided fractures that generally strike 020°–050°, oriented at ∼15°–25° obliquity to the strike of the ruptured fault surface at depth (Figures 4l and 4m). In three dimensions, the angle between mean plane in the Mountainville Fault zone east-dipping modal fracture population (036°/78°) and the mainshock nodal plane (013°/45°) is 38°. The >30°

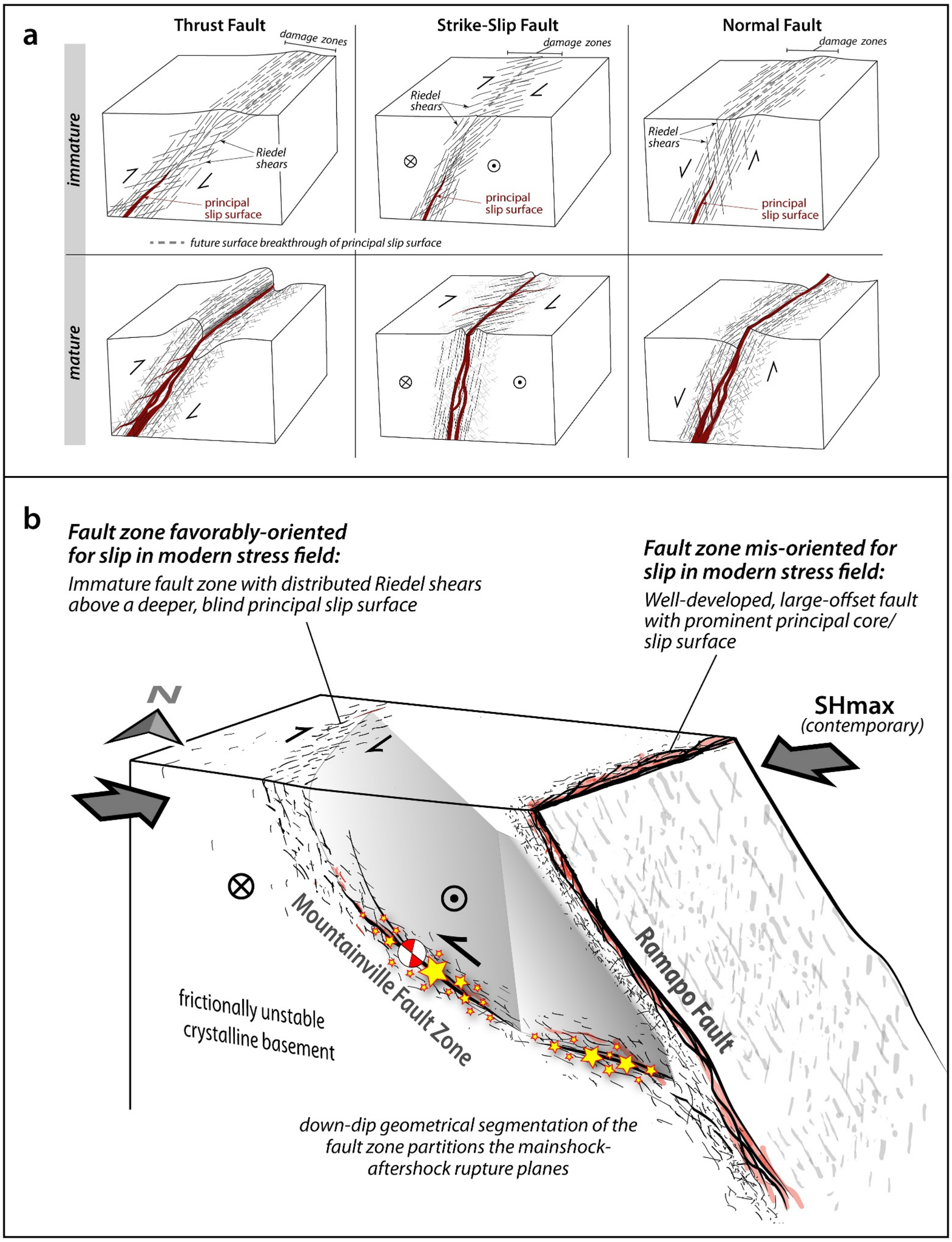

Figure 9. (a) Schematic diagram illustrating the structure of different fault types during their immature and mature phases of development (after Segall & Pollard, 1983; Faulkner et al., 2003; Blenkinsop, 2008; Mitchell & Faulkner, 2009; Faulkner et al., 2011; Gabrielsen & Braathen, 2014; Kolawole et al., 2019). (b) The structure of the Mountainville Fault Zone as informed by observations in the field exposures complimented by seismological data. The predominance of clustered shear fractures, lack of a break-through principal fault core at the surface, and the obliquity of surficial fault-fracture systems to the deeper Mw4.8 nodal plane are expected for an "immature" fault zone.

three-dimensional angular difference is likely biased by the greater population of steeply dipping fractures measured in the outcrops (Figure 4n).

The significant concentration of NNE-striking planes with high slip tendencies in the Mountainville Fault Zone which is lacking in the flanking regions (Figures 8a and 8b) suggest that slip surfaces in the fault zone are optimally-oriented with respect to the regional stress state, and that a significant population of the MF fracture planes are critically-stressed. Given the low obliquity of the field-mapped MF fracture systems to the earthquake rupture planes, we interpret that surface deformation along MF represents synthetic Riedel (R) shears above a deep-seated, blind principal core of the fault zone (i.e., principal slip surface; Figure 9b). We suggest that the relatively greater dips of the surface-mapped planes indicate an up-dip steepening of the fault zone. The poor coalescence of mapped shear fractures, lack of significant gouge accumulation, and an absence of a breakthrough principal fault core along the MF suggest that it is a low displacement fault zone. Also, the <10 km lengths of these faults are consistent with standard length-scaling of faults designated as "immature faults" in global scaling of characteristic fault parameters (Scholz, 2025; Zou & Fialko, 2024). The relocated aftershock distribution also appears to show a segmented principal slip zone of the Mountainville fault zone at depth, characterized by sections that decrease in steepness with depth (Figure 2b).

The slickensided fractures in the MF form a "stair-step" slip surface geometry as defined by the commonly cross-cutting nature of its steeply-dipping and the gently-dipping sets (e.g., Figures 4h–4k). The exposures of the Ramapo Fault show coalesced steep and gentle slip surfaces (teal line in Figure S2b in Supporting Information S1; bi-modal dip distribution in Figure S2e in Supporting Information S1) with well-developed comminuted material (breccia and gouge sheets) bounded by slickenlined surfaces (Figures S2c–S2e in Supporting Information S1). Seismic reflection imaging of the Newark Basin suggests >4 km throw on the Ramapo border fault with a long-lived Phanerozoic reactivation history from Triassic rift-related normal faulting to post-rift inversion (Ratcliffe et al., 1986; Withjack et al., 2013). Deep cores of the border fault near Tewksbury show variable dips (20°–50°E) of slip surfaces and coalesced cataclasites with thrust to oblique thrust slip vectors (Burton & Ratcliffe, 1985). At the exposures of the Ramapo Fault in Suffern, NJ, the slip vectors on both the steep and gently-dipping slip surfaces commonly document oblique thrust and minor normal slip patterns (Figure S2e in Supporting Information S1). The only observable paleo-slip vectors in the Mountainville Fault Zone show oblique-thrust (Figures 4j and 4k). The common thrust events likely represent the Mesozoic post-rift basin inversion in the rifted margin (e.g., Withjack et al., 2013). As observed at the modern-day erosional level, the internal structure of the Mountainville Fault and Ramapo Fault contrasts in terms of shear intensity (i.e., well-developed fault rocks in the latter, lacking in the former). Similar to the Ramapo Fault exposures (Figures S2b and S2e in Supporting Information S1), the mapped brittle faults in the New Jersey Highlands commonly record the post-rift thrust events (Figures 4j, 4k, 5c, and 5d, and Figures S4d–S4g in Supporting Information S1). Despite the shared kinematic history, the deformation in the Mountainville Fault Zone indicates comparatively less displacement accrual and less maturity than the Ramapo Fault. Since the Mountainville and Ramapo faults are synthetic and east-dipping, the former likely abuts against the latter at depth, defining the former as a possible footwall splay of the rift border fault (Figure 9b).

At the meter- (e.g., Figures 4h and 4i) and km-scale (Figure 2b) of observations, the poor coalescence of slip surfaces may hint at an intrinsic geometrical complexity within the fault that could cause irregularity in the propagation of slip at depth, thereby modulating the nature of earthquake rupture and strain energy release in such "immature" fault zones. This geometrical interpretation of the MF structure is highlighted by independent seismological observations. Analysis of relocated events by Beaucé et al. (2025) shows that the hypocenters define a relatively more coalesced principal slip zone at depth, however with an anomalously high *b*-value and low spatial fall-off rate that represents an immature fault with a wide damage zone at depth. The seismological analysis of aftershock behavior suggests that the fault may be a "rough" fault (Beaucé et al., 2025), consistent with our inference of fault immaturity and geometrical complexity along the fault zone.

4.2. Implications for Earthquake Hazards in Stable Continental Regions

Detailed field investigations of the geological structure of two earthquake sources in other areas of the Greater New York region reveal similar characteristics to those of the Mountainville Fault. These include the Catlin Lake Fault Zone which hosted the 1983 Mw4.7 Goodnow Earthquake near the center of the Adirondack Dome (Figure 1a; Dawers & Seeber, 1991), and the Dobbs Ferry Fault Zone which hosted the 1985 Mw3.9 Ardsley Earthquake near Dobbs Ferry just north of New York City (Figure 1b; Seeber & Dawers, 1989; Dawers & Seeber, 1991). In both regions, the causative faults manifest in outcrops as zones of distinct basement damage zones that host little or no gouge in their slip surfaces. The fault zones create subtle topographic lineaments, and locally in outcrops, the deformation zones host discontinuous but subparallel fracture clusters that strike parallel or subparallel to the mainshock nodal planes. Here in Tewksbury, the observed structural characteristics of the Mountainville Fault fit those of these structurally investigated earthquake sources. Beyond New Jersey, the

10.1029/2025JB033723

causative fault of the Mw5.1 Sparta, North Carolina earthquake exhibits significant geometrical complexity of poorly coalesced segments with variable dips and faulting styles (Neves et al., 2024). Also, based on the aftershock geometrical and productivity characteristics of the 2017 Mw4.2 Dover, Delaware earthquake, it was proposed that the causative fault is likely an immature fault (Pearson et al., 2026).

Altogether, we propose that in the highly populated US east coast, seismically unstable, immature, structurally complex faults similar to the Mountainville Fault may constitute important earthquake sources and thus, pose previously unrecognized but critical earthquake hazards. Studies demonstrate that in such regions, the lithosphere is prestressed (e.g., Craig et al., 2023; Zoback & Zoback, 1989), highlighting that local stress perturbations and the geomechanical structure of pre-existing faults may determine their susceptibility to seismic instability (Kolawole et al., 2019). The dearth of displacement accrual on many intraplate faults suggest that they are likely not accumulating elastic strain and that their seismic reactivation is likely triggered by transient stress perturbation processes (Calais et al., 2016). We expand these arguments by adding that for critically-stressed intraplate fault zone that exhibits similar "immaturity" architecture as the Mountainville Fault (Figures 9a and 9b), poor-coalescence of its slip surfaces may impose geometrical constraints and segmentation on seismic rupture. We propose that the structural complexity of critically-oriented, immature, basement-hosted fault zones (Figure 9b) may define important aspects of their seismogenesis in stable continental regions and low strain tectonic settings. Current US National Seismic Hazard Model does not include fault deformation models for the Central and Eastern US regions but is proposed to be developed for future iterations of the US seismic hazard model (Petersen et al., 2024). Similarly, probabilistic fault displacement hazard models developed for earthquake sources in Western US (e.g., Moss & Ross, 2011; Youngs et al., 2003) are lacking in the Central and Eastern US. Our results suggest that different magnitude versus rupture length scales may be required for future development of seismic hazard models that incorporate seismic source characteristics for the Eastern US.

At the regional scale of the Newark Basin in the Eastern North American rifted margin (Figure 1b), the Ramapo Fault itself is misoriented for reactivation due to its sub-parallel orientation to the SHmax (Sykes et al., 2008). Our slip tendency analysis shows that slip planes that are Ramapo Fault-parallel (i.e., NE-SW) exhibit a low tendency for reactivation, at least in the local stress field of the Tewksbury region (Figures 8a–8e). The segments of the Ramapo Fault rotate between NE-to-ENE along-strike and in a few segments strike N-S or NNE-SSW (Figure 1b), yet no recorded seismicity is collocated with the fault trace, and no Quaternary paleoseismic surface scarp is known for the fault. Rather, the observed seismicity is primarily within its footwall and is clustering on less prominent faults within its vicinity (Figure 1b). The Ramapo Fault is the border fault of the Jurassic Newark Rift basin, is mantle-rooted, and juxtaposes Grenville crystalline crust against thick sedimentary sequences (Figure 1b; Ratcliffe, 1971; Ratcliffe et al., 1986; Withjack et al., 2013). Such a large zone of lithospheric strength contrast may concentrate tectonic stresses within its vicinity as it represents a major density contrast boundary (Chisenga et al., 2023). We hypothesize a possible mechanism to explain the observed seismic clustering on immature basement faults in the Ramapo Seismic Zone. The misorientation of the Ramapo Fault to frictional failure in the current stress field allows stress to concentrate within the surrounding crust instead of the Ramapo Fault. This stress concentration may then preferentially nucleate failure on nearby secondary, less prominent faults, such as the Mountainville Fault, that are more favorably-oriented for slip in the contemporary stress field. More broadly, along-margin rotation of the regional SHmax may maintain a mis-orientation of the larger rifted margin border faults to the contemporary stress field, promoting failure of the less mature faults.

Furthermore, our friction experiments, based on the ambient tectonic loading conditions, predict stable creep at the mainshock hypocenter (positive $(a - b)$ at $\leq$5 km depth; Figure 6b) suggesting that although unsampled, concealed fault rock alterations related to frictionally unstable mineral phases may exist at depth. Thus, we speculate that a local shallow stress perturbation may have triggered the shallow mainshock event. The heterogenous composition of the Mountainville Fault rocks (Figure S5b in Supporting Information S1) may have further compounded frictional instability during fault failure by redistributing normal stresses and concentrating them preferentially on quartz-rich patches (e.g., Bedford et al., 2022; Tielke et al., 2025).

5. Conclusions

We investigated the geological and mechanical structure of the basement-hosted fault zone that generated the 5 April 2024 Mw4.8 New Jersey earthquake to advance the understanding of how fault zone structure influence intraplate seismogenesis. Our key findings in this work are as follows:

1. The up-dip projection of relocated aftershocks aligns with an area where clustered fault scarps and slickensided fractures in bedrock outcrops define a previously unmapped basement fault zone, henceforth designated as the "Mountainville Fault (MF)." The fault zone fracture clusters are gougeless and poorly coalesced, oriented at ∼15° obliquity to the mainshock nodal plane and its aftershock's best-fit plane. The fault zone lacks a breakthrough principal fault core at the surface; thus, we interpret the mapped fault-fracture clusters to be synthetic Riedel shears above a deeper, blind fault core that ruptured the 2024 event. At depth, the principal slip zone is likely more coalesced but may be characterized by sections with variable dips. Altogether, the MF structure is typical of an "immature" fault zone.
2. Laboratory friction tests on representative hypocentral rocks reveal a friction coefficient of 0.59–0.62 and a high tendency for seismic instability at lower displacement rates. The experiments predict earthquake nucleation at greater depth conditions than those of the mainshock, hinting at possible concealed fault rock alterations and/or shallow stress perturbation-driven triggering of the mainshock.
3. Using the resolved regional stress field and experimental friction coefficient as constraints, the MF's fault-fracture systems show a predominance of >90% slip tendency, confirming that the fault zone is favorably oriented to slip in the contemporary stress field
4. The observed MF characteristics are similar to those of all previously structurally investigated earthquake sources in the region and more broadly in the US East Coast, demonstrating that immature, structurally complex but critically oriented basement-hosted faults pose important seismic hazards in stable continental regions than previously thought. As such, the hazard of small faults in the east coast may be higher than previously assumed– an important consideration for future probabilistic fault displacement and deformation hazard models for the Eastern US.

Conflict of Interest

The authors declare no conflicts of interest relevant to this study.

Availability Statement

The 3-m LiDAR DEM (NJ HUNTERDON 2006) and 0.6-m Bare Earth LiDAR DEM (NJ NW6Co 2017) data used in the study can be obtained freely from the United States Geological Survey (USGS) geospatial database via the 3DEP LiDAR Explorer website (https://apps.nationalmap.gov/lidar-explorer). The fracture data supporting this study is archived on Zenodo data repository and publicly accessible at Kolawole and Foster-Baril (2024). The relocated seismic catalog plotted in this study is published in Beaucé et al. (2025). We used the ILSI software for stress inversion (v1.1.4; Beaucé, 2025).

Acknowledgments
This project is funded by the National Science Foundation Grant NSF-RAPID 2431983 awarded to Felix Waldhauser and Folarin Kolawole to support the seismology survey, field geological mapping, and laboratory friction experiments presented in this paper. We thank Maureen Chatfield for granting the team access to her property during the field mapping exercise. We thank Rachel Abercrombie, Beatrice Magnani, the handling associate editor, and two anonymous reviewers for their comments that helped to improve the quality of this paper.

References

Beaucé, E. (2025). ebeauce/ILSI: v1.1.4 [Software]. *Zenodo*. https://doi.org/10.5281/zenodo.17901517

Beaucé, E., Van Der Hilst, R. D., & Campillo, M. (2022). An iterative linear method with variable shear stress magnitudes for estimating the stress tensor from earthquake focal mechanism data: Method and examples. *Bulletin of the Seismological Society of America*, *112*(3), 1224–1239. https://doi.org/10.1785/0120210319

Beaucé, E., Waldhauser, F., Schaff, D., Kim, W. Y., & Kolawole, F. (2025). The 5 April 2024 Mw4.8 Tewksbury, New Jersey aftershock sequence resolved with machine-learning-enhanced detection methods. *Geophysical Research Letters*, *52*(12), e2024GL113598. https://doi.org/10.1029/2024gl113598

Bedford, J. D., Faulkner, D. R., & Lapusta, N. (2022). Fault rock heterogeneity can produce fault weakness and reduce fault stability. *Nature Communications*, *13*(1), 326. https://doi.org/10.1038/s41467-022-27998-2

Blanpied, M. L., Tullis, T. E., & Weeks, J. D. (1998). Effects of slip, slip rate, and shear heating on the friction of granite. *Journal of Geophysical Research*, *103*(B1), 489–511. https://doi.org/10.1029/97jb02480

Blenkinsop, T. G. (2008). Relationships between faults, extension fractures and veins, and stress. *Journal of Structural Geology*, *30*(5), 622–632. https://doi.org/10.1016/j.jsg.2008.01.008

Boyd, O. S., Barnhart, W. D., Bourke, J., Chapman, M., Earle, P. S., Huang, G. C. D., et al. (2024). Preliminary observations of the 5 April 2024 M w 4.8 New Jersey Earthquake. *The Seismic Record*, *4*(4), 240–250. https://doi.org/10.1785/0320240024

Brodsky, E. E., Gilchrist, J. J., Sagy, A., & Collettini, C. (2011). Faults smooth gradually as a function of slip. *Earth and Planetary Science Letters*, *302*(1–2), 185–193. https://doi.org/10.1016/j.epsl.2010.12.010

Burton, W. C., & Ratcliffe, N. M. (1985). Attitude, movement history, and structure of cataclastic rocks of the Flemington Fault results of core drilling near Oldwick, New Jersey (No. 1781). *US Geological Survey*.

Calais, E., Camelbeeck, T., Stein, S., Liu, M., & Craig, T. J. (2016). A new paradigm for large earthquakes in stable continental plate interiors. *Geophysical Research Letters*, *43*(20), 10–621. https://doi.org/10.1002/2016gl070815

CBS News. (2024). *New York City rocked by 1.7 magnitude earthquake suspected of causing buildings to shake*. CBS News. article by Christina Fan, Jan. 24, 2024. URL (as of 7/28/2026) Retrieved from https://www.cbsnews.com/newyork/news/fdny-responds-to-reports-of-possible-explosion-near-roosevelt-island-bridge/

Chase, B. F., Kolawole, F., Atekwana, E. A., Carpenter, B. M., Turko, M., Abdelsalam, M., & Finn, C. (2023). The 180-km-long Meers-Willow fault system in the Southern Oklahoma Aulacogen: A potential US mid-continent seismic hazard. *Bulletin*, *135*(3–4), 663–677. https://doi.org/10.1130/b36363.1

Chisenga, C., Kolawole, F., Rajaonarison, T., Atekwana, E. A., Yan, J., & Shemang, E. M. (2023). Localization of large intraplate earthquakes along faulted density-contrast boundaries: Insights from the 2017 Mw6. 5 Botswana earthquake. *Journal of African Earth Sciences*, *197*, 104752. https://doi.org/10.1016/j.jafrearsci.2022.104752

Craig, T. J., Calais, E., Fleitout, L., Bollinger, L., & Scotti, O. (2023). Time-variable strain and stress rates induced by Holocene glacial isostatic adjustment in continental interiors. *Tectonophysics*, *854*, 229815. https://doi.org/10.1016/j.tecto.2023.229815

Crone, A. J., & Wheeler, R. L. (2000). *Data for Quaternary faults, liquefaction features, and possible tectonic features in the central and eastern United States, east of the Rocky Mountain Front* (p. 342). US Department of the Interior, US Geological Survey.

Dawers, N. H., & Seeber, L. (1991). Intraplate faults revealed in crystalline bedrock in the 1983 Goodnow and 1985 Ardsley epicentral areas, New York. *Tectonophysics*, *186*(1–2), 115–131. https://doi.org/10.1016/0040-1951(91)90388-9

Dieterich, J. H. (1978). Time-dependent friction and the mechanics of stick-slip. *Pageoph*, *116*, 790–806.

Dieterich, J. H. (1979). Modeling of rock friction: 1. Experimental results and constitutive equations. *Journal of Geophysical Research*, *84*(B5), 2161–2168. https://doi.org/10.1029/jb084ib05p02161

Drake, A. A., Jr. (1984). The reading prong of New Jersey and eastern Pennsylvania-An appraisal of rock relations and chemistry of a major Proterozoic terrane in the Appalachians. In M. J. Bartholomew (Ed.), *The Grenville event in the Appalachians and related topics: Geological Society of America Special Paper* (Vol. 194, pp. 75–109).

Drake, A. A., Jr., Aleinikoff, J. N., & Volkert, R. A. (1991). The Bryram intrusive suite of the reading prong – Age and tectonic environment. *Contributions to New Jersey geology*, *1991*. https://doi.org/10.3133/b1952

Du, W. X., Kim, W. Y., & Sykes, L. R. (2003). Earthquake source parameters and state of stress for the northeastern United States and southeastern Canada from analysis of regional seismograms. *Bulletin of the Seismological Society of America*, *93*(4), 1633–1648.

Ellsworth, W. L. (2013). Injection-induced earthquakes. *Science*, *341*(6142), 1225942. https://doi.org/10.1126/science.1225942

Faulkner, D. R., Lewis, A. C., & Rutter, E. H. (2003). On the internal structure and mechanics of large strike-slip fault zones: Field observations of the Carboneras fault in southeastern Spain. *Tectonophysics*, *367*(3–4), 235–251. https://doi.org/10.1016/s0040-1951(03)00134-3

Faulkner, D. R., Mitchell, T. M., Jensen, E., & Cembrano, J. (2011). Scaling of fault damage zones with displacement and the implications for fault growth processes. *Journal of Geophysical Research*, *116*(B5), B05403. https://doi.org/10.1029/2010jb007788

Firkins, M., Kolawole, F., Marfurt, K. J., & Carpenter, B. M. (2020). Attribute-assisted characterization of basement faulting and the associated sedimentary sequence deformation in north-central Oklahoma. *Interpretation*, *8*(4), SP175–SP189. https://doi.org/10.1190/int-2020-0053.1

Foulger, G. R., Wilson, M. P., Gluyas, J. G., Julian, B. R., & Davies, R. J. (2018). Global review of human-induced earthquakes. *Earth-Science Reviews*, *178*, 438–514. https://doi.org/10.1016/j.earscirev.2017.07.008

Gabrielsen, R. H., & Braathen, A. (2014). Models of fracture lineaments—Joint swarms, fracture corridors and faults in crystalline rocks, and their genetic relations. *Tectonophysics*, *628*, 26–44. https://doi.org/10.1016/j.tecto.2014.04.022

Goldberg, D., Lupo, T., Caputi, M., Barton, C., & Seeber, L. (2003). Stress regimes in the Newark Basin rift: Evidence from core and downhole data. In P. M. LeTourneau & P. E. Olsen (Eds.), *The Great Rift Valleys of Pangea in Eastern North America, tectonics, structure, and volcanism* (Vol. 1, p. 214). Columbia Univ. Press.

Gupta, H. K. (1992). *Reservoir induced earthquakes* (p. 364). Elsevier Publishers.

Han, S., Kim, W. Y., Park, J. Y., Seo, M. S., & Kim, Y. (2024). Rupture model of the 5 April 2024 Tewksbury, New Jersey, earthquake based on regional Lg-wave data. *The Seismic Record*, *4*(3), 214–222. https://doi.org/10.1785/0320240020

Hasegawa, H. S., Wetmiller, R. J., & Gendzwill, D. J. (1989). Induced seismicity in mines in Canada—An overview. *Pure and Applied Geophysics*, *129*, 423–453.

Ikari, M. J., Marone, C., & Saffer, D. M. (2011). On the relation between fault strength and frictional stability. *Geology*, *39*(1), 83–86. https://doi.org/10.1130/g31416.1

Kim, W. Y., & Chapman, M. (2005). The 9 December 2003 central Virginia earthquake sequence: A compound earthquake in the central Virginia seismic zone. *Bulletin of the Seismological Society of America*, *95*(6), 2428–2445. https://doi.org/10.1785/0120040207

Kim, W. Y., Waldhauser, F., Beaucé, E., & Kolawole, F. (2026). Multi-segment faulting of the 5 April 2024 MW4.8 Tewksbury, New Jersey earthquake: A new paradigm for moderate-sized intraplate earthquakes. Geophysical Research Letters. In review.

Kolawole, F., & Foster-Baril, Z. (2024). Fracture data supporting: "The 2024 Mw4.8 New Jersey intraplate earthquake: Preferential rupture of an immature fault in frictionally unstable basement rocks" [Dataset]. *Zenodo*. https://doi.org/10.5281/zenodo.14104727

Kolawole, F., Johnston, C. S., Morgan, C. B., Chang, J. C., Marfurt, K. J., Lockner, D. A., et al. (2019). The susceptibility of Oklahoma's basement to seismic reactivation. *Nature Geoscience*, *12*(10), 839–844. https://doi.org/10.1038/s41561-019-0440-5

Kolawole, F., Reches, Z. E., & Carpenter, B. M. (2026). Early evolution of faults in crystalline basement by organized fracturing and damage zonation. *Journal of Structural Geology*, *208*, 105702. https://doi.org/10.1016/j.jsg.2026.105702

Kolawole, F., Turko, M. S., & Carpenter, B. M. (2020). Basement-controlled deformation of sedimentary sequences, Anadarko Shelf. *Oklahoma. Basin Research*, *32*(6), 1365–1387.

Liao, Z., Liu, H., Jiang, Z., Marfurt, K. J., & Reches, Z. E. (2017). Fault damage zone at subsurface: A case study using 3D seismic attributes and a clay model analog for the Anadarko Basin. *Oklahoma. Interpretation*, *5*(2), T143–T150. https://doi.org/10.1190/int-2016-0033.1

Magnani, M. B., Blanpied, M. L., DeShon, H. R., & Hornbach, M. J. (2017). Discriminating between natural versus induced seismicity from long-term deformation history of intraplate faults. *Science Advances*, *3*(11), e1701593. https://doi.org/10.1126/sciadv.1701593

Marone, C. (1988). Laboratory-derived friction laws and their applications to seismic faulting. *Annual Review of Earth and Planetary Sciences*, *26*, 643–696.

McGarr, A., Bekins, B., Burkardt, N., Dewey, J., Earle, P., Ellsworth, W., et al. (2015). Coping with earthquakes induced by fluid injection. *Science*, *347*(6224), 830–831. https://doi.org/10.1126/science.aaa0494

Michael, A. J. (1984). Determination of stress from slip data: Faults and folds. *Journal of Geophysical Research*, *89*(B13), 11517–11526. https://doi.org/10.1029/jb089ib13p11517

Mitchell, T. M., & Faulkner, D. R. (2009). The nature and origin of off-fault damage surrounding strike-slip fault zones with a wide range of displacements: A field study from the Atacama fault system, northern Chile. *Journal of Structural Geology*, *31*(8), 802–816. https://doi.org/10.1016/j.jsg.2009.05.002

Morris, A., Ferrill, D. A., & Henderson, D. B. (1996). Slip-tendency analysis and fault reactivation. *Geology*, *24*(3), 275–278. https://doi.org/10.1130/0091-7613(1996)024<0275:staafr>2.3.co;2

Moss, R. E. S., & Ross, Z. E. (2011). Probabilistic fault displacement hazard analysis for reverse faults. *Bulletin of the Seismological Society of America*, *101*(4), 1542–1553. https://doi.org/10.1785/0120100248

Neves, M., Chuang, L. Y., Li, W., Peng, Z., Figueiredo, P. M., & Ni, S. (2024). Complex rupture dynamics of the extremely shallow August 2020 M5.1 Sparta, North Carolina earthquake. *Communications Earth & Environment*, *5*(1). https://doi.org/10.1038/s43247-024-01316-8

Patel, S., Kolawole, F., Walter, J. I., Chen, X., & Marfurt, K. J. (2021). Seismic illumination of small-throw seismogenic faults, Anadarko Basin. *Oklahoma. Interpretation*, *9*(2), SE35–SE51. https://doi.org/10.1190/int-2020-0135.1

Pearson, K. M., Lekic, V., & Wagner, L. (2026). Low aftershock productivity and fault geometry of the 2017 Delaware earthquake. *Seismological Research Letters*, *97*(2A), 957–976. https://doi.org/10.1785/0220250322

Petersen, M. D., Shumway, A. M., Powers, P. M., Field, E. H., Moschetti, M. P., Jaiswal, K. S., et al. (2024). The 2023 US 50-state national seismic hazard model: Overview and implications. *Earthquake Spectra*, *40*(1), 5–88. https://doi.org/10.1177/87552930231215428

Rankin, D. W., Drake, A. A., Jr., & Ratcliffe, N. M. (1989). Geologic map of the U.S. Appalachians showing the Laurentian margin and Taconic orogen. In R. D. Hatcher Jr., W. A. Thomas, & G. W. Viele (Eds.), *The Appalachian Ouachita Orogen, U.S. (the geology of North America, v. F-2)*. Geological Society of America. scale 1:1,500,000.

Ratcliffe, N. M. (1971). The Ramapo fault system in New York and adjacent northern New Jersey: A case of tectonic heredity. *Geological Society of America Bulletin*, *82*(1), 125–142. https://doi.org/10.1130/0016-7606(1971)82[125:trfsin]2.0.co;2

Ratcliffe, N. M., Burton, W. C., D'angelo, R. M., & Costair, J. K. (1986). Low-angle extensional faulting, reactivated mylonites, and seismic reflection geometry of the Newark basin margin in eastern Pennsylvania. *Geology*, *14*(9), 766–770. https://doi.org/10.1130/0091-7613(1986)14<766:lefrma>2.0.co;2

Rice, J. R., & Ruina, A. L. (1983). Stability of steady frictional slipping. *Journal of Applied Mechanics*, *50*(2), 343–349. https://doi.org/10.1115/1.3167042

Rimando, J. M., & Peace, A. L. (2021). Reactivation potential of intraplate faults in the western Quebec seismic zone, eastern Canada. *Earth and Space Science*, *8*(8), e2021EA001825. https://doi.org/10.1029/2021ea001825

Ruina, A. (1983). Slip instability and state variable friction laws. *Journal of Geophysical Research*, *88*(B12), 10359–10370. https://doi.org/10.1029/jb088ib12p10359

Sagy, A., & Brodsky, E. E. (2009). Geometric and rheological asperities in an exposed fault zone. *Journal of Geophysical Research*, *114*(B2). https://doi.org/10.1029/2008jb005701

Scholz, C. H. (2025). The correspondence of earthquakes and faults. *Earth and Space Science*, *12*(8), e2025EA004217. https://doi.org/10.1029/2025ea004217

Seeber, L., Armbruster, J. G., Kim, W. Y., Barstow, N., & Scharnberger, C. (1998). The 1994 Cacoosing Valley earthquakes near Reading, Pennsylvania: A shallow rupture triggered by quarry unloading. *Journal of Geophysical Research*, *103*(B10), 24505–24521. https://doi.org/10.1029/98jb01497

Seeber, L., & Dawers, N. (1989). Characterization of an intraplate seismogenic fault in the Manhattan Prong, Westchester Co., NY. *Seismological Research Letters*, *60*(2), 71–78. https://doi.org/10.1785/gssrl.60.2.71

Seeber, L., Ekström, G., Jain, S. K., Murty, C. V. R., Chandak, N., & Armbruster, J. G. (1996). The 1993 Killari earthquake in central India: A new fault in Mesozoic basalt flows? *Journal of Geophysical Research*, *101*(B4), 8543–8560. https://doi.org/10.1029/95jb01865

Segall, P., & Pollard, D. D. (1983). Nucleation and growth of strike slip faults in granite. *Journal of Geophysical Research*, *88*(B1), 555–568. https://doi.org/10.1029/jb088ib01p00555

Skarbek, R. M., & Savage, H. M. (2019). RSFit3000: A MATLAB GUI-based program for determining rate and state frictional parameters from experimental data. *Geosphere*, *15*(5), 1665–1676. https://doi.org/10.1130/ges02122.1

Sykes, L. R. (1978). Intraplate seismicity, reactivation of preexisting zones of weakness, alkaline magmatism, and other tectonism postdating continental fragmentation. *Reviews of Geophysics*, *16*(4), 621–688. https://doi.org/10.1029/rg016i004p00621

Sykes, L. R., Armbruster, J. G., Kim, W. Y., & Seeber, L. (2008). Observations and tectonic setting of historic and instrumentally located earthquakes in the greater New York City–Philadelphia Area. *Bulletin of the Seismological Society of America*, *98*(4), 1696–1719. https://doi.org/10.1785/0120070167

Tarantola, A., & Valette, B. (1982). Generalized nonlinear inverse problems solved using the least squares criterion. *Reviews of Geophysics*, *20*(2), 219–232. https://doi.org/10.1029/rg020i002p00219

Tielke, J., Verdecchia, A., Pederson, C., Prakash, A., McCarthy, C., Kolawole, F., & Harrington, R. M. (2025). Hybrid frictional behavior of hydrothermally-altered fault zones in long-lived polyphase geothermal reservoirs. *Geophysical Research Letters*, *52*, e2025GL117709. https://doi.org/10.1029/2025GL117709

Vavryčuk, V. (2014). Iterative joint inversion for stress and fault orientations from focal mechanisms. *Geophysical Journal International*, *199*(1), 69–77. https://doi.org/10.1093/gji/ggu224

Volkert, R. A. (2021). *Bedrock geologic map of the Califon quadrangle Hunterdon and Morris counties*. United State Geological Survey OPEN-FILE MAP OFM 133.

Wheeler, R. L., & Crone, A. J. (2001). Known and suggested quaternary faulting in the midcontinent United States. *Engineering Geology*, *62*(1–3), 51–78. https://doi.org/10.1016/s0013-7952(01)00050-3

Withjack, M. O., Schlische, R. W., Malinconico, M. L., & Olsen, P. E. (2013). Rift-basin development: Lessons from the Triassic–Jurassic Newark Basin of eastern North America. In W. U. Mohriak, A. Danforth, P. J. Post, D. E. Brown, G. C. Tari, M. Nemčok, et al. (Eds.), *Conjugate divergent margins (Geological Society, London, Special Publications)* (Vol. 369(1), pp. 301–321). Geological Society, London. https://doi.org/10.1144/sp369.13

Youngs, R. R., Arabasz, W. J., Anderson, R. E., Ramelli, A. R., Ake, J. P., Slemmons, D. B., et al. (2003). A methodology for probabilistic fault displacement hazard analysis (PFDHA). *Earthquake Spectra*, *19*(1), 191–219. https://doi.org/10.1193/1.1542891

Zoback, M. L., & Zoback, M. D. (1989). Tectonic stress field of the continental United States. In L. C. Pakiser & W. D. Mooney (Eds.), *Geophysical framework of the continental United States: Boulder, Colorado* (p. 172). Geological Society of America Memoir.

Zou, X., & Fialko, Y. (2024). Can large strains be accommodated by small faults: "Brittle flow of rocks" revised. *Earth and Space Science*, *11*(11), e2024EA003824. https://doi.org/10.1029/2024ea003824

References From the Supporting Information

Aljubran, M. J., & Horne, R. N. (2024). Thermal Earth model for the conterminous United States using an interpolative physics-informed graph neural network. *Geothermal Energy*, *12*(1), 25. https://doi.org/10.1186/s40517-024-00304-7

10.1029/2025JB033723

Goldberg, D., Reynolds, D., Williams, C., Witte, W. K., Olsen, P. E., & Kent, D. V. (1994). Well logging results from the Newark Rift Basin Coring Project. *Scientific Drilling*, *4*(4–6), 267–279.

Samuelson, J., & Spiers, C. J. (2012). Fault friction and slip stability not affected by CO_2 storage: Evidence from short-term laboratory experiments on North Sea reservoir sandstones and caprocks. *International Journal of Greenhouse Gas Control*, *11*, S78–S90. https://doi.org/10.1016/j.ijggc.2012.09.018